Letter

60° and 120° domain walls in epitaxial $BaTiO_3$(111)/Co multiferroic heterostructures

Kévin J. A. Franke [1], Colin Ophus [2], Andreas K. Schmid [2], and Christopher H. Marrows [1,*]

[1]*School of Physics and Astronomy, University of Leeds, Leeds LS2 9JT, United Kingdom*

[2]*National Center for Electron Microscopy, Molecular Foundry, Lawrence Berkeley National Laboratory, Berkeley, California 94720, USA*

(Received 11 November 2021; revised 9 December 2022; accepted 31 March 2023; published 19 April 2023)

We report on domain pattern transfer from a ferroelectric $BaTiO_3$ substrate with a (111) orientation of the surface to an epitaxial Co film grown on a Pd buffer layer. Spatially modulated interfacial strain transfer from ferroelectric/ferroelastic domains and inverse magnetostriction in the ferromagnetic film induce stripe regions with a modulation of the in-plane uniaxial magnetic anisotropy direction. Using spin-polarized low-energy electron microscopy, we observe the formation of two distinct anisotropy configurations between stripe regions, leading to angles of 60° or 120° between the magnetizations of adjacent domains. Moreover, through application of a magnetic field parallel or perpendicular to these stripes, head-to-head or head-to-tail magnetization configurations are initialized. This results in four distinct magnetic domain-wall types associated with different energies and domain widths, which, in turn, affects whether domain pattern transfer can be achieved.

DOI: 10.1103/PhysRevB.107.L140407

Multiferroic heterostructures are often used to modify and control the properties of ferromagnetic films via interfacial coupling to a ferroelectric substrate [1–6]. Imprinting of ferroelectric domain patterns into ferromagnetic thin films has been achieved, for example, via exchange coupling from (001)-oriented multiferroic $BiFeO_3$ [2,7,8]. Alternatively, interfacial strain transfer from ferroelectric/ferroelastic domains in tetragonal (001)-oriented $BaTiO_3$ induces spatially modulated magnetoelastic anisotropies in ferromagnetic thin films. Domain pattern transfer is achieved when the induced anisotropy overcomes intrinsic properties of the ferromagnetic film [9–12]. As a result, magnetic domain walls are strongly pinned onto their ferroelectric counterparts, which has been used to drive magnetic domain-wall motion with an applied voltage [13,14]. Applied magnetic fields can tune magnetic domain-wall properties, such as their width and chirality [14–16].

Previously, domain-wall coupling between (001)-oriented $BaTiO_3$ substrates exhibiting a_1-a_2 domains (where the polarization rotates by 90° between domains) and in-plane magnetized thin films has been investigated extensively [15–17]. The magnetization in the pinned ferromagnetic domain walls rotates by 90° giving rise to two distinct domain-wall types [15]: after the application of a saturating magnetic field perpendicular to the stripes, magnetically uncharged head-to-tail domain walls are formed. The domain-wall width is determined by a competition between the uniaxial magnetic anisotropy and the short-range exchange interaction.

Magnetically charged head-to-head domain walls are formed after demagnetizing parallel to the stripes. The domain-wall width is now determined by a competition between the magnetic anisotropy and long-range magnetostatics. The charged domain walls have been shown to be orders of magnitude wider than the uncharged domain walls, their width increasing linearly with film thickness (unlike uncharged domain walls) [16,18]. Domain pattern transfer breaks down when the width of domain walls becomes comparable to the width of the anisotropy stripe regions. This breakdown occurs for different stripe widths and film thicknesses depending on which type of domain wall is initialized.

Here, we investigate the imprinting of the ferroelectric domains of (111)-oriented $BaTiO_3$ substrates into epitaxial Co films through a Pd buffer layer. Using spin-polarized low-energy electron microscopy (SPLEEM), we are able to investigate at which point in the sample preparation domain-pattern transfer occurs. We show that four distinct domain-wall types can be stabilized, and explore their effect on domain pattern transfer as a function of film thickness.

SPLEEM allows for high-resolution imaging of magnetic contrast combined with *in situ* thin-film deposition [19,20]. Magnetic contrast is obtained because the amount of electrons backscattered elastically from the sample surface depends on the relative orientation of the spin polarization of the incident electrons and the sample magnetization. The spin polarization of the incident electron beam can be precisely oriented in any spatial direction allowing for control over the direction of magnetic contrast. Under the imaging conditions used, we estimate the resolution of the SPLEEM to be ∼100 nm, and so the micron-scale domain patterns that we study here are well resolved. Our thin films are deposited *in situ* at room temperature by molecular beam epitaxy in a chamber with a pressure in the 10^{-11} mbars range.

Figure 1(a) shows the domain pattern observed after depositing 4 nm of Co. Double-headed arrows indicate the

*c.h.marrows@leeds.ac.uk

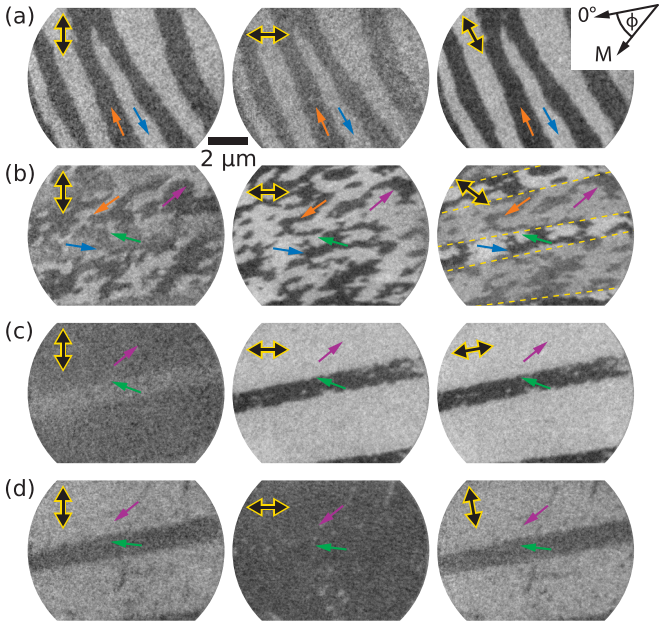

FIG. 1. Evolution of magnetic domain pattern and magnetization orientation in 4-nm-thick Co: (a) As-deposited film. (b) After heating to 350 °C and returning to room temperature. (c) After applying a saturating magnetic field perpendicular and (d) parallel to the stripe domain orientation. Double-headed arrows indicate the axis of magnetic contrast and single-headed arrows the local orientation of the magnetization. The sketch in the upper right corner defines the in-plane angle ϕ between the local magnetization direction and the axis of sensitivity of the SPLEEM.

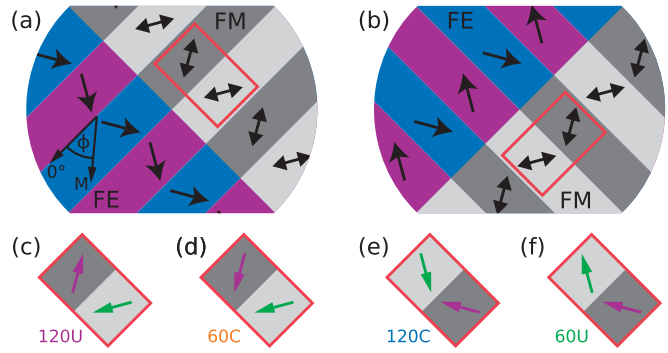

FIG. 2. Sketches of ferroelectric (blue/magenta) and magnetic anisotropy (light/dark gray) domain patterns for a Co film strain coupled to a $BaTiO_3$ (111) substrate corresponding to (a) quasiparallel and (b) quasiperpendicular anisotropy patterns. The negative magnetostriction of the Co means that the easy axes of the anisotropy domains in the Co are orthogonal to the polarization in the ferroelectric domains of the BTO. (c)–(f) Possible orientations of the magnetization in the domains leading to four distinct magnetic domain-wall structures.

in-plane magnetic contrast axis, whereas arrows show the orientation of the magnetization in the domains. The observed pattern corresponds to a demagnetized domain pattern where adjacent stripe domains are separated by 180° domain walls.

After heating to 350 °C, a temperature that is above the ferroelectric phase transition at 120 °C in the $BaTiO_3$ but still well below the 1100 °C bulk ferromagnetic Curie point for Co, the domain pattern shown in Fig. 1(b) is observed at room temperature. It took about 20 min to heat the sample and 30 min for it to cool again. The magnetization now aligns along uniaxial directions that rotate by 60° between stripe regions, which is particularly clear in the rightmost image. This observation indicates the presence of a uniaxial anisotropy that rotates by 60° between adjacent anisotropy stripe regions.

After saturating the magnetization perpendicular to these stripes, the magnetization aligns with these anisotropy directions as shown in Fig. 1(c). There is a head-to-tail configuration of the magnetization in adjacent stripes. We determined the in-plane angle ϕ of the magnetization within each domain by using the same method as in Ref. [21]: by measuring the SPLEEM contrast as a function of angle of the spin polarization of the beam. We then fitted a cosine function to that data and used a value returned by that fit along with its error bar as the value of ϕ in that domain.

The magnetization in the wider stripes (violet arrow) makes a $29 \pm 2°$ angle with the domain wall, whereas the magnetization in the narrow stripe (green arrow) is rotated $32 \pm 3°$ away from the domain wall. The spin rotation $\Delta\phi = |\phi_1 - \phi_2|$, defined as the difference in magnetization between neighboring stripes is, therefore, $\Delta\phi = 119 \pm 4°$.

Figure 1(d) shows the domain pattern observed after saturating the magnetization parallel to the stripe domains. The magnetization in neighboring stripes is now oriented head to head. The magnetization in the wide stripes has been rotated by exactly 180°, and still makes an angle of $29 \pm 2°$ with the domain wall. The magnetization in the narrow central domain has not flipped, but now makes an angle of only $14 \pm 2°$ with the domain wall. The spin rotation is reduced to $43 \pm 3°$.

We will now show that these results can be explained by interfacial strain transfer from the (111)-oriented $BaTiO_3$ substrate owing to inverse magnetostriction in the Co film, which we refer to as a domain imprinting process. At room temperature, $BaTiO_3$ is in its tetragonal phase where the cubic parent phase is elongated by 1.1% along a ⟨001⟩ direction. This elongation coincides with a ferroelectric polarization that points in the same direction. From investigations of (001)-oriented $BaTiO_3$ substrates, it is known that strain relaxation leads to the formation of ferroelectric stripe domains where the polarization rotates by 90° between neighboring domains (see, for example, Ref. [15]) since it prefers to point along the ⟨001⟩ axes. When these axes are projected onto the (111) surface, they form sets of three [22] that have in-plane components that are 120° apart. This results in an angle of 60° between the lattice elongation in adjacent stripe domains since each corresponds to one of the two possible threefold sets of axes. One resulting projection of the ferroelectric polarization onto the (111) surface is sketched in blue/magenta in Fig. 2(a) where the in-plane component of polarization rotates by 60° between stripe domains.

If the associated lattice elongation is transferred to a thin film with negative magnetostriction as in the case of Co [23], it results in the uniaxial anisotropy pattern sketched in gray in which the easy axes lie orthogonal to the polarization in the underlying ferroelectric domains. Note that only the in-plane component of the elongation of the substrate lattice can

impose a strain on a thin film, whereas the out-of-plane component cannot. Thus, the anisotropy easy axes make a ±30° angle with the domain boundaries. For convenience we will, thus, refer to the anisotropy pattern sketched in Fig. 2(a) as "quasiparallel." The "quasiperpendicular" anisotropy pattern sketched in Fig. 2(b) where the anisotropies make a ±60° angle with the domain boundaries will be discussed later.

When the magnetization aligns with the uniaxial anisotropies of the quasiparallel configuration, two distinct types of magnetic domain wall can be formed as sketched in Figs. 2(c) and 2(d): the magnetization can be initialized in a head-to-head (or equivalent tail-to-tail) configuration with a spin rotation of $\Delta\phi = 60°$. Lines of magnetic flux cannot be drawn continuously over this domain wall, and so this leads to a net accumulation of magnetic charges. The domain wall is, thus, labeled 60C for its spin rotation and the fact that it is magnetically charged. Alternatively, a head-to-tail configuration of the magnetization with $\Delta\phi = 120°$ can be formed, yielding a domain wall labeled 120U as it does not exhibit a net magnetic charge (uncharged) since magnetic flux lines are continuous over the domain wall. Both domain walls are of the Néel type since the axis about which the magnetization rotates, assuming on magnetostatic grounds that there is never an out-of-plane magnetization component, is normal to the film plane. Hence, this axis lies on the plane of the domain wall, which is the definition of the Néel configuration [24]. (In contrast, a Bloch wall is defined by this rotation axis lying normal to the domain wall.) These two configurations closely resemble the orientations of the magnetization observed in Figs. 1(c) and 1(d). The only discrepancy is observed for the magnetization in the narrow central domain in the 60C configuration as it makes a $14 \pm 2°$ angle with the domain wall instead of the expected angle of 30°.

We investigate this reduction in angle using micromagnetic simulations and thereby determine the strength of the uniaxial anisotropy induced in the Co film. We use OOMMF [25] to simulate a 4-nm-thick magnetic film with typical values for Co of saturation magnetization $M_s = 1.46 \times 10^6$ A/m and exchange stiffness $A = 3.1 \times 10^{-11}$ J/m [24]. These assumptions are necessary since *ex situ* measurements of these properties are impossible in this case, owing to the fact that the capping layer that would be needed would introduce a new interface that would be very likely modify them from their *in situ* values in an unknown way. Close inspection of the images in Fig. 1 reveals that the width of the central domain varies from 0.9 to 1.1 μm. Ferroelectric domain walls are known to not be perfectly parallel. We, thus, simulate a 7 μm wide area with a central narrow stripe surrounded by two wide stripes. The uniaxial easy axis is along $\phi_1 = -30°$ in the narrow central domain, and along $\phi_2 = 30°$ in the wide domains. Two-dimensional boundary conditions are used to simulate an extended film [26]. We vary the width of the narrow domain and the strength of the uniaxial anisotropy.

In Fig. 3(a), the resulting magnetization angle in the central domain for the head-to-head magnetization configuration is compared to the experimental observation. From this comparison, we find a match of the magnetization angle for an uniaxial anisotropy constant $K_u = (1 \pm 0.2) \times 10^4$ J/m^3. This value is reasonable for a system of this type [15]. For 120U domain

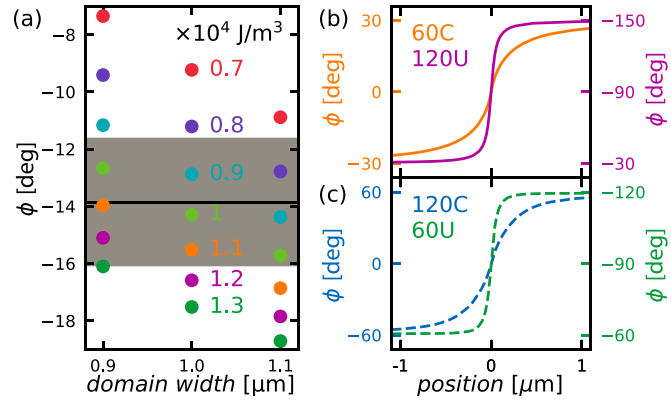

FIG. 3. (a) Determination of the anisotropy strength from the magnetization orientation in Fig. 1(d). The width of the central domain ranges from 0.9 to 1.1 μm. The experimentally determined magnetization angle (black line, error in gray) is compared to the magnetization angle obtained from micromagnetic simulations for anisotropy strengths ranging from 0.7 to 1.3×10^4 J/m^3 (colored dots). (b) and (c) Magnetization profiles of all four magnetic domain-wall types.

walls, the magnetization in the central domain aligns with the uniaxial anisotropy axis along $\phi_1 = -30°$ both for the experimental observation and for the micromagnetic simulations in the anisotropy range considered here (not shown).

We now turn our attention to the origin of this reduction in spin rotation. As the magnetization in wide domains is seen to align with the easy axis, we repeat the micromagnetic simulations for an anisotropy constant $K_u = 1 \times 10^4$ J/m^3, but now, for anisotropy stripes of equal width of 4 μm. We show the resulting magnetic domain wall profiles in Fig. 3(b). Despite having a smaller spin rotation, the accumulation of magnetic charges in the 60C magnetic domain wall leads to a more gradual rotation of the magnetization, and, therefore, a wider domain wall, than for the 120U magnetic domain wall. Even 1 μm from the magnetic domain-wall center the magnetization of the 60C magnetic domain wall has not fully aligned with the anisotropy axis. As the domain walls in Fig. 1(d) are only 1 ± 0.1 μm apart, the magnetization can never fully align with the anisotropy axis because the tails of domain walls overlap.

For the ferroelectric polarization orientations sketched in Fig. 2(a), the domain configuration sketched in Fig. 2(b) is, in principle, energetically equivalent. When the in-plane lattice elongation associated with this ferroelectric/ferroelastic domain pattern is transferred to the Co film, inverse magnetostriction is expected to induce the anisotropy pattern schematically shown in gray, and labeled quasiperpendicular. It is distinct from the quasiparallel anisotropy stripe pattern as can be seen from the type of magnetic domain walls that are obtained when the magnetization aligns with the anisotropy directions: after saturating the magnetization parallel to the domain walls, 120C magnetic domain walls are obtained, whereas 60U magnetic domain walls are initialized after saturation perpendicular to the domain boundaries [Figs. 2(e) and 2(f)]. The angular profiles of these domain walls are shown in Fig. 3(c), confirming that the width of domain walls depends significantly on the magnetostatic energy and less on the spin

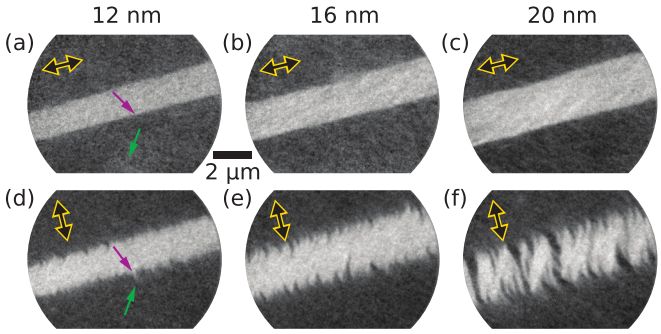

FIG. 4. Magnetic domain configurations for quasiperpendicular anisotropy domain wall as a function of film thickness.

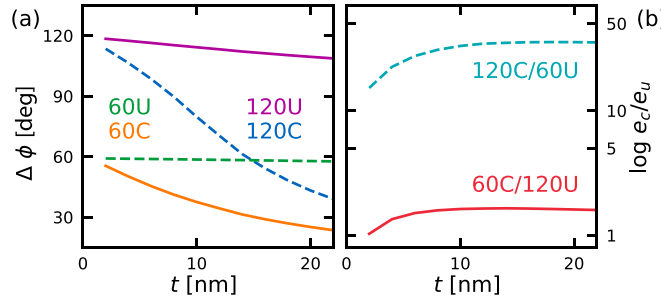

FIG. 5. Dependence of (a) the spin rotation $\Delta\phi$, and (b) the ratio between energy densities as a function of magnetic film thickness t for 2.5-μm-wide anisotropy stripes.

rotation. We show experimental evidence for these domain walls in Fig. 4.

These images were taken on a second sample that was prepared in the same manner as the one imaged in Fig. 1 except that a 12-nm-thick Co film was grown. We observe that after annealing and appropriate demagnetization, a 60U magnetic domain wall is imaged in Fig. 4(a), whereas a 120C magnetic domain wall is depicted in Fig. 4(d). For similar reasons to those given above, the 60U wall will have the Néel structure whereas the 120C wall will have the Bloch structure. We have, therefore, observed all four possible magnetic domain-wall types sketched in Fig. 2.

We continue by investigating the film thickness dependence of the magnetic domain configurations for quasiperpendicular anisotropy domain walls. As the SPLEEM instrument allows for *in situ* thin film deposition, the film thickness can easily be increased and images taken at the same position. After each additional thin-film deposition, the sample is annealed to ensure strain transfer throughout the thin film. The ferroelectric domain pattern is expected to be reinitialized during the annealing process, but ferroelectric domain walls tend to be pinned by defects, strains (imposed by the holder), and the shape of the substrate are all expected to have an influence on the ferroelectric domain pattern and location of ferroelectric domain walls [27–31]. Fortunately, as seen in Figs. 4(b) and 4(c), the domain pattern does not change significantly after increasing the film thickness to 16 and 20 nm. A widening of the central domain is observed.

Note that the 60U magnetic domain walls observed in panels (a)–(c) of Fig. 4 are sharp and straight. In contrast, the charged domain wall depicted in panels (d)–(f) of that figure is a zig-zag wall, thus, avoiding the accumulation of magnetic charges. At 20 nm [panel (f)], this even leads to the formation of magnetic stripe domains within the central anisotropy stripe. As described before, such a behavior is not observed for 60U magnetic domain walls. Clearly, the energy cost of forming a charged magnetic domain wall over an uncharged one increases with film thickness as expected.

We again investigate this further using micromagnetic simulations of 2.5-μm-wide anisotropy stripes of equal width. Note that the width of the central stripe in Fig. 4 ranges from 1.5 μm at $t = 12$ nm to 2.5 μm at $t = 20$ nm. The use of two-dimensional periodic boundary conditions and the fact that simulations do not take into account defects in the film precludes the formation of magnetic domains within anisotropy stripes. This makes it easier to compare the different types of magnetic domain walls.

Figure 5(a) shows the spin rotation $\Delta\phi$ as a function of thickness for all four domain-wall types. Although little change is observed for both types of uncharged domain walls, charged domain walls exhibit a clear reduction of their spin rotation in thicker films. The trend can be understood from the expected thickness dependence of domain-wall widths. Although the width of uncharged domain walls is expected to be independent of the film thickness, the accumulation of a net magnetic charge at the domain wall leads to a linear dependence of the domain-wall width on the film thickness. In the latter case, a thicker film, therefore, results in a larger overlap of neighboring domain walls, and, in turn, to a reduction in spin rotation.

Figure 5(b) shows the ratio between energy densities of domain patterns with charged and uncharged magnetic domain walls. We see that for 2-nm-thick films, the 120C configuration that we attempted to initialize in Fig. 4(d) is 15 times higher in energy than the corresponding uncharged (60U) domain configuration. For a 20-nm-thick film this ratio increases to 35, making 120C magnetic domain walls energetically very costly. As a result, we observe the roughening of magnetic domain walls for thin magnetic films in Fig. 4(d) and the breakdown of pattern transfer and formation of magnetic domains within anisotropy stripe domains for thicker films [Fig. 4(f)]. In comparison, the energy cost of forming 60C domain walls over 120U ones in a quasiparallel anisotropy pattern (depicted in Fig. 1) is much lower.

So far, we have attributed the formation of magnetic stripe domains observed in Figs. 1 and 4 to coupling of the ferromagnetic thin films to the (111)-oriented $BaTiO_3$ substrates via interfacial strain transfer and inverse magnetostriction. Although our data strongly support this interpretation, we are unable to image the ferroelectric $BaTiO_3$ domains in SPLEEM, and are, thus, unable to definitely observe a one-to-one correlation of ferroelectric and ferromagnetic domains. We are, however, able to provide further evidence for our claim.

As described earlier, when heated $BaTiO_3$ undergoes a transition from a tetragonal to a cubic phase at around 120 °C [32]. The strain imposed on the ferromagnetic thin film and the induced uniaxial anisotropy are, thus, expected to vanish at the phase transition. Figure 6 shows a series of SPLEEM images taken as a function of temperature. The first image is

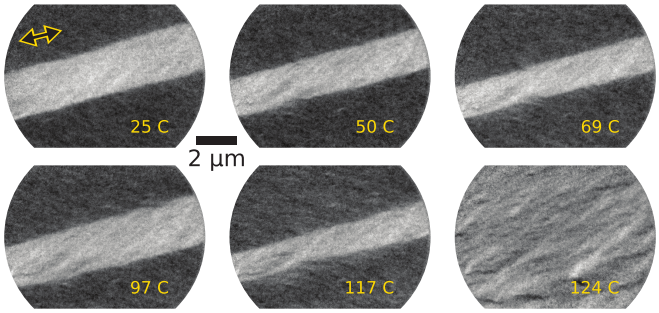

FIG. 6. Evolution of 60U domain pattern as a function of temperature.

the same as the one in Fig. 4(c), hence, shows 60U magnetic domain-wall configuration in a 20-nm Co film. Images are taken in exactly the same location. The change in width of the central domain as a function of temperature is, therefore, not an artifact, and the upper domain wall moves with temperature. We can only speculate about the origin of this movement, but a temperature-activated motion of ferroelectric domain walls between local pinning sites or a change in internal stresses of the constrained substrate seem likely [31,33]. Most importantly, the magnetic stripe pattern disappears between the images collected at 117° C and 124° C, exactly where the ferroelectric phase transition of $BaTiO_3$ occurs, confirming that magnetic stripe domains are formed via coupling to the substrate in its tetragonal phase.

We now discuss how this new heterostructure holds the potential of unprecedented electric-field tuning of magnetic domain walls. So far, the application of an electric field along the [001] direction of a $BaTiO_3$ substrate exhibiting a_1-a_2 domains eventually yields a switch of the polarization and associated lattice elongation towards the out-of-plane direction. As a result the spatial modulation of strain that allows for domain pattern transfer to a ferromagnetic thin film is lost [34].

In (111)-oriented $BaTiO_3$ substrates, the polarization makes an angle of $\approx 54.7°$ with the surface normal. In the tetragonal phase, the application of an electric field in the out-of-plane direction cannot switch the polarization into the [111] direction. Instead, the lattice is deformed, which would modulate the strain imposed onto the ferromagnetic film and, therefore, alter the magnitude of the anisotropy constant. This, in turn, affects the width of magnetic domain walls. Moreover, the application of larger electric fields yields a transition to an orthorhombic phase, with the same symmetry of induced anisotropy directions but reduced anisotropy constant. Finally, a second transition to rhombohedral phase at even larger fields aligns the polarization with the electric-field direction, and spatial modulations of strain would be erased [22,35].

Domain patterns are ubiquitous in many disparate materials systems [36]. Our results are reflected in other coupled order parameter systems. For instance, superconducting vortex nucleation can be controlled by means of underlying ferromagnetic domains [37] or, vice versa, ferromagnetic domains have been imprinted using superconducting vortices [38].

To summarize, we have demonstrated domain pattern transfer from (111)-oriented $BaTiO_3$ substrates to epitaxial Co films via spatially modulated interfacial strain transfer and inverse magnetostriction. Two types of anisotropy patterns can be induced in the ferromagnetic film, and magnetic fields can be used to initialize magnetically charged or uncharged domain walls with a spin rotation of 60° or 120°. In our samples, pattern transfer occurs only after annealing through the ferroelectric phase transition, indicating strain relaxation in the Pd buffer layer. We expect that these multiferroic heterostructures can be used for electric-field tuning of magnetic domain walls and pattern transfer in novel spintronic devices.

Data associated with this publication are available from Research Data Leeds at [39].

This project has received funding from the European Union's Horizon 2020 Research and Innovation Programme under the Marie Skłodowska-Curie Grant Agreement No. 750147. K.J.A.F. acknowledges support from the Jane and Aatos Erkko Foundation. Work at the Molecular Foundry was supported by the Office of Science, Office of Basic Energy Sciences of the U.S. Department of Energy under Contract No. DE-AC02-05CH11231. This research used the lawrencium computational cluster resource provided by the IT Division at the Lawrence Berkeley National Laboratory (Supported by the Director, Office of Science, Office of Basic Energy Sciences of the U.S. Department of Energy) under Contract No. DE-AC02-05CH11231.

[1] D. Lebeugle, A. Mougin, M. Viret, D. Colson, and L. Ranno, Electric Field Switching of the Magnetic Anisotropy of a Ferromagnetic Layer Exchange Coupled to the Multiferroic Compound $BiFeO_3$, Phys. Rev. Lett. **103**, 257601 (2009).

[2] Y.-H. Chu, L. W. Martin, M. B. Holcomb, M. Gajek, S.-J. Han, Q. He, N. Balke, C.-H. Yang, D. Lee, W. Hu, Q. Zhan, P.-L. Yang, A. Fraile-Rodríguez, A. Scholl, S. X. Wang, and R. Ramesh, Electric-field control of local ferromagnetism using a magnetoelectric multiferroic, Nature Mater. **7**, 478 (2008).

[3] L. You, B. Wang, X. Zou, Z. S. Lim, Y. Zhou, H. Ding, L. Chen, and J. Wang, Origin of the uniaxial magnetic anisotropy in $La_{0.7}Sr_{0.3}MnO_3$ on stripe-domain $BiFeO_3$, Phys. Rev. B **88**, 184426 (2013).

[4] M. Ghidini, F. Maccherozzi, X. Moya, L. C. Phillips, W. Yan, J. Soussi, N. Métallier, M. E. Vickers, N. J. Steinke, R. Mansell, C. H. W. Barnes, S. S. Dhesi, and N. D. Mathur, Perpendicular local magnetization under voltage control in Ni films on ferroelectric $BaTiO_3$ substrates, Adv. Mater. **27**, 1460 (2015).

[5] M. Ghidini, F. Ye, N.-J. Steinke, R. Mansell, C. H. W. Barnes, and N. D. Mathur, Non-volatile voltage control of in-plane and out-of-plane magnetization in polycrystalline Ni films on ferroelectric PMN-PT $(001)_{pc}$ substrates, J. Appl. Phys. **129**, 154101 (2021).

[6] J. Chen and S. Dong, Manipulation of Magnetic Domain Walls by Ferroelectric Switching: Dynamic Magnetoelectricity at the Nanoscale, Phys. Rev. Lett. **126**, 117603 (2021).

[7] M. Trassin, J. D. Clarkson, S. R. Bowden, J. Liu, J. T. Heron, R. J. Paull, E. Arenholz, D. T. Pierce, and J. Unguris, Interfacial coupling in multiferroic/ferromagnet heterostructures, Phys. Rev. B **87**, 134426 (2013).

[8] G. De Luca, P. Schoenherr, J. Mendil, D. Meier, M. Fiebig, and M. Trassin, Domain-Pattern Transfer across an Artificial Magnetoelectric Interface, Phys. Rev. Appl. **10**, 054030 (2018).

[9] T. Lahtinen, J. Tuomi, and S. van Dijken, Pattern transfer and electric-field-induced magnetic domain formation in multiferroic heterostructures, Adv. Mater. **23**, 3187 (2011).

[10] T. H. E. Lahtinen, Y. Shirahata, L. Yao, K. J. A. Franke, G. Venkataiah, T. Taniyama, and S. van Dijken, Alternating domains with uniaxial and biaxial magnetic anisotropy in epitaxial Fe films on $BaTiO_3$, Appl. Phys. Lett. **101**, 262405 (2012).

[11] R. Streubel, D. Köhler, R. Schäfer, and L. M. Eng, Strain-mediated elastic coupling in magnetoelectric nickel/barium-titanate heterostructures, Phys. Rev. B **87**, 054410 (2013).

[12] Y. Shirahata, R. Shiina, D. L. González, K. J. A. Franke, E. Wada, M. Itoh, N. A. Pertsev, S. van Dijken, and T. Taniyama, Electric-field switching of perpendicularly magnetized multilayers, NPG Asia Materials **7**, e198 (2015).

[13] K. J. A. Franke, B. Van de Wiele, Y. Shirahata, S. J. Hämäläinen, T. Taniyama, and S. van Dijken, Reversible Electric-Field-Driven Magnetic Domain-Wall Motion, Phys. Rev. X **5**, 011010 (2015).

[14] D. López González, Y. Shirahata, B. Van de Wiele, K. J. A. Franke, A. Casiraghi, T. Taniyama, and S. van Dijken, Electric-field-driven domain wall dynamics in perpendicularly magnetized multilayers, AIP Adv. **7**, 035119 (2017).

[15] K. J. A. Franke, T. H. E. Lahtinen, and S. van Dijken, Field tuning of ferromagnetic domain walls on elastically coupled ferroelectric domain boundaries, Phys. Rev. B **85**, 094423 (2012).

[16] K. J. A. Franke, D. López González, S. J. Hämäläinen, and S. van Dijken, Size Dependence of Domain Pattern Transfer in Multiferroic Heterostructures, Phys. Rev. Lett. **112**, 017201 (2014).

[17] A. Casiraghi, T. Rincón Domínguez, S. Rößler, K. J. A. Franke, D. López González, S. J. Hämäläinen, R. Frömter, H. P. Oepen, and S. van Dijken, Influence of elastically pinned magnetic domain walls on magnetization reversal in multiferroic heterostructures, Phys. Rev. B **92**, 054406 (2015).

[18] A. Hubert, Charged walls in thin magnetic films, IEEE Trans. Magn. **15**, 1251 (1979).

[19] K. Grzelakowski and E. Bauer, A flange-on type low energy electron microscope, Rev. Sci. Instrum. **67**, 742 (1996).

[20] N. Rougemaille and A. K. Schmid, Magnetic imaging with spin-polarized low-energy electron microscopy, Eur. Phys. J. Appl. Phys. **50**, 20101 (2010).

[21] K. J. A. Franke, C. Ophus, A. K. Schmid, and C. H. Marrows, Competition between exchange and magnetostatic energies in domain pattern transfer from $BaTiO_3$(111) to a Ni thin film, Phys. Rev. Mater. **7**, 034403 (2023).

[22] S. Wada, S. Suzuki, T. Noma, T. Suzuki, M. Osada, M. Kakihana, S.-E. Park, L. E. Cross, and T. R. Shrout, Enhanced piezoelectric property of barium titanate single crystals with engineered domain configurations, Jpn. J. Appl. Phys. **38**, 5505 (1999).

[23] P. McCorkle, Magnetostriction and magnetoelectric effects in iron, nickel and cobalt, Phys. Rev. **22**, 271 (1923).

[24] J. M. D. Coey, *Magnetism and Magnetic Materials* (Cambridge University Press, Cambridge, UK, 2010).

[25] M. Donahue and D. Porter, *OOMMF User's Guide, Version 1.0*, Interagency Report NISTIR 6376 (National Institute of Standards and Technology, Gaithersburg, MD, 1999).

[26] W. Wang, C. Mu, B. Zhang, Q. Liu, J. Wang, and D. Xue, Two-dimensional periodic boundary conditions for demagnetization interactions in micromagnetics, Comput. Mater. Sci. **49**, 84 (2010).

[27] P. W. Forsbergh, Domain structures and phase transitions in barium titanate, Phys. Rev. **76**, 1187 (1949).

[28] E. A. Little, Dynamic behavior of domain walls in barium titanate, Phys. Rev. **98**, 978 (1955).

[29] J. M. noz Saldaña, G. Schneider, and L. Eng, Stress induced movement of ferroelastic domain walls in $BaTiO_3$ single crystals evaluated by scanning force microscopy, Surf. Sci. **480**, L402 (2001).

[30] I. A. Luk'yanchuk, A. Schilling, J. M. Gregg, G. Catalan, and J. F. Scott, Origin of ferroelastic domains in free-standing single-crystal ferroelectric films, Phys. Rev. B **79**, 144111 (2009).

[31] A. K. Tagantsev, L. E. Cross, and J. Fousek, *Domains in Ferroic Crystals and Thin Films* (Springer, New York, NY, 2010).

[32] H. Kay and P. Vousden, XCV. symmetry changes in barium titanate at low temperatures and their relation to its ferroelectric properties, Lond. Edinb. Dublin philos. mag. j. sci. **40**, 1019 (1949).

[33] T. Mitsui and J. Furuichi, Domain structure of Rochelle salt and KH_2PO_4, Phys. Rev. **90**, 193 (1953).

[34] K. J. A. Franke, T. H. E. Lahtinen, A. Casiraghi, D. López González, S. J. Hämäläinen, and S. van Dijken, Electric field control of magnetism based on elastically coupled ferromagnetic and ferroelectric domains, *Nanoscale Ferroelectrics and Multiferroics* (Wiley, Hoboken, NJ, 2016), Chap. 21, pp. 677–699.

[35] A. J. Bell, Phenomenologically derived electric field-temperature phase diagrams and piezoelectric coefficients for single crystal barium titanate under fields along different axes, J. Appl. Phys. **89**, 3907 (2001).

[36] M. Seul and D. Andelman, Domain shapes and patterns: The phenomenology of modulated phases, Science **267**, 476 (1995).

[37] M. Iavarone, S. A. Moore, J. Fedor, V. Novosad, J. A. Pearson, and G. Karapetrov, Influence of domain width on vortex nucleation in superconductor/ferromagnet hybrid structures, J. Supercond. Nov. Magn. **28**, 1107 (2015).

[38] A. Sander, G. Orfila, D. Sanchez-Manzano, N. Reyren, M. A. Mawass, F. Gallego, S. Collin, K. Bouzehouane, K. Höflich, F. Kronast, F. Grilli, A. Rivera-Calzada, J. Santamaria, J. E. Villegas, and S. Valencia, Superconducting imprint of magnetic textures in ferromagnets with perpendicular magnetic anisotropy, Sci. Rep. **11**, 20788 (2021).

[39] https://doi.org/10.5518/1327